

Classification of stable Dirac and Weyl semimetals with reflection and rotational symmetry

Zihao Gao^{1,*}, Meng Hua^{1,*}, Haijun Zhang², Xiao Zhang^{1,†}

1. Department of Physics, Sun-Yat-Sen University, Guangzhou, China and

2. National Laboratory of Solid State Microstructures, School of Physics,

Collaborative Innovation Center of Advanced Microstructures, Nanjing University,

Nanjing 210093, China. *These authors contributed equally to this work. †Correspondence and requests for materials should be addressed to Xiao Zhang (email: yngweiz@gmail.com).

(Dated: August 11, 2015)

Three dimensional (3D) Dirac semimetal is a novel state of quantum matter, characterized by the gapless bulk four-fold degeneracy near Fermi energy. Soon after its discovery, the classification of stable 3D Dirac semimetals with inversion and rotational symmetry have been studied. However, only ten out of thirty-two point groups have both inversion and rotational symmetry, and we need a more complete classification of stable 3D Dirac semimetals. Here we classify stable 3D Dirac semimetals with reflection symmetry and rotational symmetry in the presence of time reversal symmetry, which belong to seventeen different point groups. These systems include the systems preserving inversion symmetry except C_{3i} . They have two classes of reflection symmetry, with the mirror plane parallel to rotation axis and the mirror plane perpendicular to rotation axis. In both cases two types of Dirac semimetals are determined by four different reflection symmetries. The first type of Dirac semimetals will appear through accidental band crossing (ABC). The second type of Dirac semimetals have a Dirac point at a time reversal invariant momentum (TBC). We show that in both mirror parallel and perpendicular cases, $C_{2,3}$ symmetry can only protect stable Dirac points via TBC, while $C_{4,6}$ symmetry can have stable Dirac points as ABC or TBC. We further discuss that Weyl line nodes and Dirac semimetal can exist in Brillouin zone at the same time using C_{4v} symmetry as an example. Finally we classify Dirac line nodes and Weyl line nodes to show in which types of mirror plane they can exist.

I. INTRODUCTION

Dirac semimetals are new states of quantum matter. They have gap closing (Dirac points or Dirac line nodes) of conduction band and valence band which show pseudorelativistic physics of 3-dimensional (3D) Dirac fermions near the Fermi energy. Before the discovery of Dirac semimetals, the topological quantum states, such as topological insulator [1–4] and graphene [5, 6], can have 2-dimensional (2D) Dirac fermions. Different from topological insulators and superconductors, Dirac semimetals hold nontrivial features in the bulk states [7–14]. When the systems reach a quantum critical point between normal insulator and topological insulator, the accidental crossing of inverted bands will generate Dirac points in bulk [15].

To realize Dirac semimetal we can tune the chemical composition to the critical point of quantum phase transition [15], however those Dirac points are not stable. Soon stable 3D Dirac semimetals have been theoretically predicted [9, 16] and observed experimentally in Cd_3As_2 and Na_3Bi [17–21] by Angle-resolved photoemission spectroscopy (ARPES). In these materials there are two stable Dirac points in k_z axis stabilized by rotational symmetry. While in β -cristobalite structure such like BiO_2 [7], the Dirac points exist at a time reversal invariant momentum (TRIM). The unique electronic band structures of Dirac semimetals make them have unusual high mobility, oscillating quantum spin hall effect (QSHE) and giant diamagnetism [19]. Recently, a new type of Dirac semimetal, with Dirac line nodes (DLN), has been proposed in Cu_3NPd [10, 14] and

LaN [22]. DLN can exist in the system with or without spin-orbit coupling (SOC) [23]. At the same time, theoretical prediction shows that time reversal symmetry (TRS) breaking systems including $HgCr_2Se_4$ [24] has Weyl nodes and a Weyl line node (WLN) in its mirror plane. Also systems with TRS breaking such as pyrochlore iridates [25] and $(CdO)_2(EuO)_2$ [26] or with TRS such as TaAs, NbAs, NbP and TaP [27–37] have Weyl nodes.

Inspired by these work, we ask the question that which point group can protect Dirac semimetals. Yang and Nagaosa have classified Dirac points in physical systems preserving inversion symmetry [38]. However, only ten out of thirty-two point groups have both inversion and rotational symmetry, and we need a more complete classification of stable 3D Dirac points. Meanwhile, considering the critical role that reflection symmetry plays in newly predicted DLN and WLN semimetals, a classification of them by reflection symmetry becomes necessary as well. Here we classify 3D stable Dirac points in the systems preserving TRS, reflection symmetry and uniaxial rotational symmetry. Known that the reflection symmetry plays an important role in classification of topological phases [39, 40], we first study the classification of reflection symmetries in space groups. Apart from point group C_{3i} , all the other point groups preserving inversion symmetry are covered in our discussion. Then we show that four different reflection symmetries can protect two different types of Dirac semimetals, Dirac semimetals created by ABC or by TBC. We further discuss the coexistence of Dirac points and Weyl line nodes through $k \cdot p$ theory using C_{4v} symmetry as an example. Finally we classify DLN and WLN to show in which types of mirror

plane they can exist.

II. RESULTS

Consider four energy bands which could be generated in a system preserving time reversal symmetry (TRS) and uniaxial rotational symmetry, we can describe them through a 4×4 Hamiltonian in a very general form,

$$H = \begin{pmatrix} h_{\uparrow\uparrow}(\vec{k}) & h_{\uparrow\downarrow}(\vec{k}) \\ h_{\downarrow\uparrow}(\vec{k}) & h_{\downarrow\downarrow}(\vec{k}) \end{pmatrix} = \sum_{i,j=0}^3 a_{ij}(\vec{k}) \tau_i \sigma_j$$

where σ_i represents the spin space and τ_i represents orbital space. $h_{\sigma\sigma'}$ ($\sigma = \uparrow, \downarrow$) is a 2×2 matrix and $\uparrow\downarrow$ represent opposite spin in k_z direction. All the $a_{ij}(\vec{k})$ are real functions and we can determine the parity of each coefficient $a_{ij}(\vec{k})$ through TRS $H(-\vec{k}) = TH(\vec{k})T^{-1}$, where $T = i\sigma_y K$. The system is invariant under C_n rotational symmetry which gives $C_n H(\vec{k}) C_n^{-1} = H(R_n \vec{k})$, where R_n is a rotation operator for 3D n-fold rotation in k-space and the basis are chosen to be eigenstates of C_n . We choose the rotation axis as k_z axis, therefore $R_n k_z = k_z$. Rotational symmetry suggests commutation relation $C_n H(k_z) C_n^{-1} = H(k_z)$ in k_z between the Hamiltonian $H(k_z)$ and C_n operators. Therefore we choose a set of bases to make C_n a diagonal form $C_n = \text{diag}(\alpha_p, \alpha_q, \alpha_r, \alpha_s)$, where $\alpha_p = \exp[i\frac{2\pi}{n}(p + \frac{1}{2})]$, p is the angular momentum for point group rotational symmetry and the effective angular momentum for a screw rotation. Here each basis is a C_n rotation eigenstate and has a definite rotation eigenvalue $p + \frac{1}{2}$. In the presence of TRS, C_n has only two independent basis whose rotation eigenvalues are α_p and α_q (see Appendix).

After applying TRS and rotational symmetry, the Hamiltonian in k_z axis becomes a diagonal form with the above basis

$$H(k_z) = a_{00} + a_{03}\sigma_3 + a_{33}\tau_3\sigma_3 + a_{30}\tau_3 \quad (1)$$

The Dirac points are created only when $a_{03,33,30}(k_z, m) = 0$, where m is a control parameter. There are three equations and two variables, so we need additional symmetry constraints to guarantee these equations having at least one solution that can generate stable Dirac points. We impose reflection symmetry into the systems with uniaxial rotational symmetry and TRS, and show the conditions where Dirac points exist.

II.1. Classification of reflection symmetry

Among the point groups, the reflection symmetries can be distinguished in two classes by the relative positions between mirror plane and rotation axis k_z . In the first class, k_z axis parallels the mirror plane, and the system doesn't preserve inversion symmetry which correspond to point groups $C_{2v}, C_{3v}, C_{4v}, C_{6v}, D_{2d}$ and T_d . In these

systems, reflection symmetry can be a point group symmetry as shown in FIG. 1.(a₁) or a nonsymmorphic glide plane symmetry which is the combination of a reflection and a translation t as shown in FIG. 1.(a₂). Neupane et. al[17] realized Dirac semimetal on Cd₃As₂ which belongs to nonsymmorphic space group $I4_1cd$ (C_{4v}). Whereas in the second class, when k_z axis is perpendicular to the mirror plane, inversion symmetry will emerge through the combination of reflection symmetry and C_2, C_4 or C_6 rotational symmetry[38, 41]. Here the point group reflection symmetry is shown in FIG. 1.(a₃) and the glide plane symmetry in nonsymmorphic space group is shown in FIG. 1.(a₄).

Mirror operator is an inversion operation followed by a C_2 rotation whose rotation axis perpendicular to the mirror plane. It should satisfy the following constraints: (1)[M, T] = 0, (2) $M^+M = 1$, (3) $MM = e^{i\phi}$. If we set mirror plane as yz -plane or xy -plane, the reflection symmetry operator will have the form: (A) $M_k = \pm\tau_0 \otimes i\sigma_k$, (B) $M_k = \pm\tau_z \otimes i\sigma_k$, (C) $M_k = \pm\tau_x \otimes i\sigma_k$ and (D) $M_k = \pm i\tau_y \otimes i\sigma_k$ ($k = x, z$, see Appendix), among which (C, D) represent glide mirror symmetry. For example, with the basis containing only equivalent sites[see FIG. 1.(a₁)] $|P_{A+\uparrow}\rangle, |P_{A-\uparrow}\rangle, |P_{A-\downarrow}\rangle, |P_{A+\downarrow}\rangle$, a reflection operation along yz -plane writes $M_x = -\tau_0 \otimes i\sigma_x$. And if we set the basis as $|P_{A+\downarrow}\rangle, |P_{B+\downarrow}\rangle, -|P_{A-\uparrow}\rangle, -|P_{B-\uparrow}\rangle$, where A/B are two inequivalent sites for the same kind of atom [FIG. 1.(a₂)], then the reflection operation along yz -plane with an additional interchanging of A and B sites writes $M_x = \tau_x \otimes i\sigma_x$ (see Appendix). Note that the basis in our framework is the single atom basis after considering spin-orbit coupling (SOC).

Owing to the TRS and rotational symmetry, the Hamiltonian in k_z axis has been constrained as Eq. (1). After we impose reflection symmetry, the $H(k_z)$ can be further constrained and will reveal Dirac semimetal phase. As shown in Appendix, different mirror operator will hold different type of Dirac semimetal. When the mirror operator is $M_k = \tau_0/\tau_z \otimes \sigma_k$ ($k = x, z$), only $a_{30}(k_z, m)$ survives. $a_{30}(k_z)$ is an even function respect to k_z , so $a_{30}(k_z, m) \approx M_0 - M_1 k_z^2$ for the leading order. Two Dirac points will emerge in the k_z axis at $k_z = \pm\sqrt{M_0/M_1}$. This kind of Dirac semimetal is created through the two bands accidentally crossing each other when the conduction band and valence band have different rotation eigenvalues ($p \neq q$). It can be understood as a phase between normal insulator and weak topological insulator[42, 43]/topological crystalline insulator[44, 45] [FIG. 1.(b)]. When mirror operator is $M_k = i\tau_y/\tau_x \otimes \sigma_k$, only $a_{33}(k_z, m)$ survives which is an odd function respect to k_z . The leading order is $a_{33} = M_2 k_z$. There is one Dirac point at TRIM generated by band crossing (TBC). Under this scenario, the Dirac points are created and stabilized by the crystalline symmetry [FIG. 1.(c)(d)]. We will use tables below to show the physical properties of all kinds of Dirac semimetals.

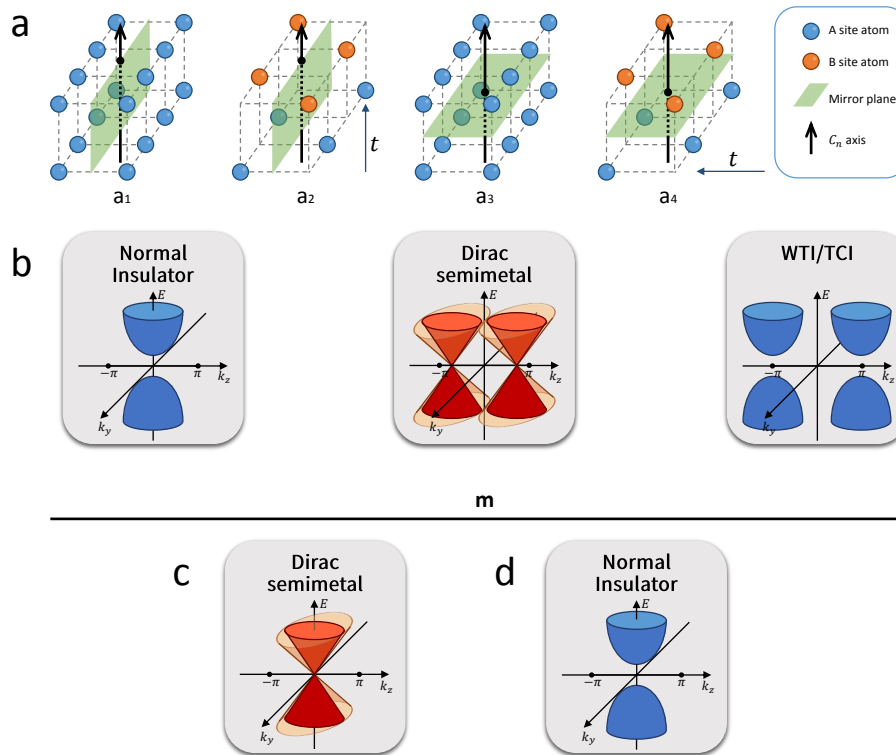


FIG. 1. (a) There are four kinds of reflection symmetries in space groups: the mirror plane parallel to rotation axis as shown in a_1 and a_2 and the mirror plane perpendicular to rotation axis as shown in a_3 and a_4 . In both cases, for normal mirror plane a_1 and a_3 , there is only one equivalent site. As for glide mirror plane a_2 and a_4 , which is a reflection symmetry with a t translation, there are two inequivalent sites in the lattice. (b), (d) correspond to the Dirac points of type ABC and TBC in TABLE I and TABLE II respectively. (b) The phase transition determined by a control parameter m and Dirac semimetal created by ABC. When m is in a proper range, two Dirac points show up on k_z axis. This phase lays between two gapped phases such as normal insulator and weak topological insulator (WTI) and topological crystalline insulator (TCI). (c) The Dirac semimetal phase is protected by crystalline symmetry. In this case, Dirac point can be found at TRIM. (d) When the conduction band and valence band have the same rotation eigenvalue, i.e. $p = q$, they will never cross each other because of strong level repulsion.

II.2. Classification table

If we impose reflection symmetry, TRS and rotational symmetry to the Hamiltonian in k_z axis, we will have the criteria for basis's rotational eigenvalues to obtain Dirac semimetal phase. The classification of Dirac semimetals when the mirror plane is parallel to k_z axis is shown in TABLE I. C_2 and C_3 rotational systems can only generate Dirac points via TBC. C_4 and C_6 symmetries can protect Dirac semimetal phase in the presence of all those four reflection symmetries.

The classification of 3D Dirac semimetals when the mirror plane is perpendicular to k_z axis is demonstrated in TABLE II. Inversion symmetry can emerge through $P = C_2 m_z$, where C_2 is a two-fold rotation along k_z axis in systems preserving C_2, C_4, C_6 symmetry. Yang and

Nagaosa [38] have already considered unitary inversion operator $P = \tau_0, \tau_x, \tau_z$. We show that in TABLE II the same results hold when inversion operators are unitary. However, the mirror operators can also generate the antiunitary inversion operator $P = i\tau_y$. $P = i\tau_y$ is an inversion operator with a translation in nonsymmorphic space group. It will produce a phase factor after being applied twice. One special case is the D_{3h} group, which does not involve inversion symmetry. As shown in TABLE III, only $M_z = i\tau_y \otimes \sigma_z$ can protect a Dirac point at TRIM with the combination of rotation eigenvalues $p = 2, q = 0$ or $p = 2, q = 1$.

TABLE I. Classification table when k_z is parallel to mirror plane. Dirac semimetals can be obtained in the systems with reflection and C_n rotational symmetry. Here we choose k_z as the rotation axis and assume that yz -plane is a mirror plane. (p, q, r, s) can be regarded as a set of orbital angular momentum in z direction and j is the total angular momentum. For example, for $(p, q, r, s) = (3, 2, 0, 1)$ in C_4 system, the C_4 rotation eigenvalues are $(e^{i\frac{7\pi}{4}}, e^{i\frac{5\pi}{4}}, e^{i\frac{\pi}{4}}, e^{i\frac{3\pi}{4}})$, which equal $(e^{-i\frac{1}{2}\frac{\pi}{2}}, e^{-i\frac{3}{2}\frac{\pi}{2}}, e^{i\frac{1}{2}\frac{\pi}{2}}, e^{i\frac{3}{2}\frac{\pi}{2}})$. For compact presentation, we assume $n/2 \leq q \leq p < n$ and consider the equivalence between $\{p, r\}$ and $\{q, s\}$. The leading order of $f_{\pm}, g_{\pm}, g_0 + g_z, g_0 - g_z$ are shown in the table. Each term should be multiplied by a coefficient function of k_z respecting to the parity of $a_{ij}(k)$ when constructing the elements of the Hamiltonian. The bulk Dirac points are obtained through ABC when $M_x = \pm\tau_0/\tau_z \otimes \sigma_x$ and they are obtained through TBC when $M_x = \pm\tau_x/i\tau_y \otimes \sigma_x$. The material Cd_3As_2 belongs to space group $I4_1cd$ [17].

M_x	C_n	(p,q,r,s)	Total j	f_{\pm}	g_{\pm}	$g_0 + g_z$	$g_0 - g_z$	Dirac Type	Materials	Dispersion in k_y direction
$\pm\tau_0/\tau_z$	C_2	-	-	-	-	-	-	-	-	-
	C_3	-	-	-	-	-	-	-	-	-
	C_4	(3,2,0,1)	$(\pm\frac{1}{2}, \pm\frac{3}{2})$	k_+	k_{\pm}^2	k_-	k_+	ABC	$\text{Cd}_3\text{As}_2(I4_1cd)$	Linear Dirac
	C_6	(5,4,0,1)	$(\pm\frac{1}{2}, \pm\frac{3}{2})$	k_+	k_{\pm}^2	k_-	k_{\pm}^3	ABC		Linear Dirac
	C_6	(5,3,0,2)	$(\pm\frac{1}{2}, \pm\frac{5}{2})$	k_{\pm}^2	k_{\pm}^3	k_-	k_+	ABC		Linear Dirac
	C_6	(4,3,1,2)	$(\pm\frac{3}{2}, \pm\frac{5}{2})$	k_+	k_{\pm}^2	k_{\pm}^3	k_+	ABC		Linear Dirac
$\pm\tau_x$	C_2	-	-	-	-	-	-	-	-	-
	C_3	(2,1,0,1)	$(\pm\frac{1}{2}, \pm\frac{3}{2})$	k_+	k_+	k_-	k_+k_-	TBC	-	Linear Dirac
	C_4	(3,2,0,1)	$(\pm\frac{1}{2}, \pm\frac{3}{2})$	k_+	k_{\pm}^2	k_-	k_+	TBC	-	Linear Dirac
	C_6	(5,4,0,1)	$(\pm\frac{1}{2}, \pm\frac{3}{2})$	k_+	k_{\pm}^2	k_-	k_{\pm}^3	TBC	-	Linear Dirac
	C_6	(5,3,0,2)	$(\pm\frac{1}{2}, \pm\frac{5}{2})$	k_{\pm}^2	k_{\pm}^3	k_-	k_+	TBC	-	Linear Dirac
	C_6	(4,3,1,2)	$(\pm\frac{3}{2}, \pm\frac{5}{2})$	k_+	k_{\pm}^2	k_{\pm}^3	k_+	TBC	-	Linear Dirac
$\pm i\tau_y$	C_2	(1,1,0,0)	$(\pm\frac{1}{2}, \pm\frac{1}{2})$	k_+k_-	k_+	k_{\pm}	k_{\pm}	TBC	-	Linear Dirac
	C_3	(2,2,0,0)	$(\pm\frac{1}{2}, \pm\frac{1}{2})$	k_+k_-	k_-	k_-	k_-	TBC	-	Linear Dirac
	C_3	(2,1,0,1)	$(\pm\frac{1}{2}, \pm\frac{3}{2})$	k_+	k_+	k_-	k_+k_-	TBC	-	Linear Dirac
	C_4	(3,3,0,0)	$(\pm\frac{1}{2}, \pm\frac{1}{2})$	k_+k_-	k_-	k_-	k_-	TBC	-	Linear Dirac
	C_4	(3,2,0,1)	$(\pm\frac{1}{2}, \pm\frac{3}{2})$	k_+	k_{\pm}^2	k_-	k_+	TBC	-	Linear Dirac
	C_4	(2,2,1,1)	$(\pm\frac{3}{2}, \pm\frac{3}{2})$	k_+k_-	k_+	k_+	k_+	TBC	-	Linear Dirac
	C_6	(5,5,0,0)	$(\pm\frac{1}{2}, \pm\frac{1}{2})$	k_+k_-	k_-	k_-	k_-	TBC	-	Linear Dirac
	C_6	(5,4,0,1)	$(\pm\frac{1}{2}, \pm\frac{3}{2})$	k_+	k_{\pm}^2	k_-	k_{\pm}^3	TBC	-	Linear Dirac
	C_6	(5,3,0,2)	$(\pm\frac{1}{2}, \pm\frac{5}{2})$	k_{\pm}^2	k_{\pm}^3	k_-	k_+	TBC	-	Linear Dirac
	C_6	(4,4,1,1)	$(\pm\frac{3}{2}, \pm\frac{3}{2})$	k_+k_-	k_{\pm}^3	k_{\pm}^3	k_{\pm}^3	TBC	-	Quadratic Dirac
	C_6	(4,3,1,2)	$(\pm\frac{3}{2}, \pm\frac{5}{2})$	k_+	k_{\pm}^2	k_{\pm}^3	k_+	TBC	-	Linear Dirac
	C_6	(3,3,2,2)	$(\pm\frac{5}{2}, \pm\frac{5}{2})$	k_+k_-	k_+	k_+	k_+	TBC	-	Linear Dirac

II.3. The coexistence of Dirac points and Weyl line nodes

For now we can construct Dirac points in the systems preserving reflection symmetry but without inversion symmetry. It is known that breaking inversion symmetry can produce Weyl points or Weyl line nodes. So we expect in some cases Dirac points and Weyl line nodes can exist simultaneously with SOC. We illustrate this distinctive properties in materials with C_{4v} point group like Cd_3As_2 through $k \cdot p$ perturbation method (see Appendix). Note that we choose mirror operator as $m_x = \tau_z \otimes i\sigma_x$ with $p=3, q=2, r=0, s=1$ corresponding to the 3rd row of TABLE I. The detailed calculations are shown in Appendix. By choosing some proper parameters, the band structure shown in FIG. 2.(a) exhibits two Dirac points along $\Gamma - Z$ direction and two Weyl line nodes in yz -plane and xz -plane. FIG. 2.(b) shows the phase transition between different topological phases.

Obviously the phase transition of Weyl line nodes is independent of the emergence of Dirac points in k_z direction[FIG. 2.(c)]. The simultaneous appearance of Dirac points and Weyl line nodes indicates a new class of topological phase with time reversal symmetry and SOC.

As illustrated in FIG. 2.(a) this $k \cdot p$ Hamiltonian can have different topological phases. These phases depend on the SOC term D_0 and inversion breaking term B_0 . FIG. 2.(b) shows the phase diagram respecting to B_0 and D_0 . There are two different phases when changing parameters. In the gray area, the systems break inversion symmetry but can not protect Weyl semimetal. In the dark blue area, the conduction band and valence band will cross to form a Weyl line node with $A_0 = -0.06eV$. When $A_0 = -0.00922eV$ the dark blue area extend to the light blue area. When the inversion breaking term $B_0 \approx 0$, the system will not have Weyl line nodes phase on the D_0 axis, but it can protect Dirac semimetal phase just like in $\text{Cd}_3\text{As}_2(I4_1cd)$. This phase diagram is inde-

TABLE II. Classification table when k_z is perpendicular to mirror plane. Dirac semimetals can be obtained in the systems with C_n rotational symmetry and reflection symmetry. Here we choose k_z as the rotation axis and assume that xy -plane is a mirror plane. (p, q, r, s) can be regarded as a set of orbital angular momentum in z . For example, for $(p, q, r, s) = (2, 0, 1, 3)$ in C_4 system, the C_4 rotation eigenvalues are $(e^{i\frac{5\pi}{4}}, e^{i\frac{1\pi}{4}}, e^{i\frac{3\pi}{4}}, e^{i\frac{7\pi}{4}})$, which equal $(e^{-i\frac{3}{2}\frac{\pi}{2}}, e^{i\frac{1}{2}\frac{\pi}{2}}, e^{i\frac{3}{2}\frac{\pi}{2}}, e^{-i\frac{1}{2}\frac{\pi}{2}})$. j is the total angular momentum. For compact presentation, we assume $q \leq p < n$ and consider the equivalence between $\{p, r\}$ and $\{q, s\}$. The leading order of $f_{\pm}, g_{\pm}, g_0 + g_z, g_0 - g_z$ are shown in the table. Each term should be multiplied by an coefficient function of k_z respecting to the parity of $a_{ij}(k)$ when constructing the elements of the Hamiltonian. The bulk Dirac points are obtained through ABC when $M_z = \pm\tau_0/\tau_z \otimes \sigma_z$ and they are obtained through TBC when $M_z = \pm\tau_x/i\tau_y \otimes \sigma_z$. The material Cd_3As_2 belongs to space group $I4_1acd$.

M_z	C_2	P	C_n	(p,q,r,s)	Total j	f_{\pm}	g_{\pm}	$g_0 \pm g_z$	Dirac type	Materials	Dispersion in k_y		
τ_0/τ_z	τ_0		C_2	-	-	-	-	-	-	-	-	-	
			C_4	(2,0,1,3)	$(\pm\frac{3}{2}, \pm\frac{1}{2})$	k_{\pm}^2	k_+	0	ABC	$\text{Cd}_3\text{As}_2(I4_1acd)$	Linear		
			C_6	(2,0,3,5)	$(\pm\frac{5}{2}, \pm\frac{1}{2})$	k_+^2	k_{\pm}^3	0	ABC		Quadratic		
			C_6	(3,1,2,4)	$(\pm\frac{5}{2}, \pm\frac{3}{2})$	k_+^2	k_-	0	ABC		Linear		
			C_6	(4,0,1,5)	$(\pm\frac{3}{2}, \pm\frac{1}{2})$	k_-^2	k_-	0	ABC		Linear		
	C_2	-	-	-	-	-	-	-	-				
	τ_z/τ_0			C_4	(1,0,2,3)	$(\pm\frac{3}{2}, \pm\frac{1}{2})$	k_+	k_{\pm}^2	0	ABC	-	Linear	
				C_6	(1,0,4,5)	$(\pm\frac{3}{2}, \pm\frac{1}{2})$	k_+	k_+^2	0	ABC	-	Linear	
				C_6	(2,1,3,4)	$(\pm\frac{5}{2}, \pm\frac{3}{2})$	k_+	k_-^2	0	ABC	-	Linear	
				C_6	(3,0,2,5)	$(\pm\frac{5}{2}, \pm\frac{1}{2})$	k_{\pm}^3	k_-^2	0	ABC	-	Quadratic	
C_2/C_6				-	-	-	-	-	-	-	-	-	
$i\tau_y$	τ_0	$i\tau_y$	C_2/C_6	-	-	-	-	-	-	-	-		
			C_4	(2,0,1,3)	$(\pm\frac{3}{2}, \pm\frac{1}{2})$	k_{\pm}^2	k_-	k_+	TBC	-	Linear		
	τ_z	τ_x		C_2	(1,0,0,1)	$(\pm\frac{1}{2}, \pm\frac{1}{2})$	k_{\pm}	0	k_{\pm}	TBC	Distorted spinels[46]	Linear	
				C_4	-	-	-	-	-	-		-	-
				C_6	(3,0,2,5)	$(\pm\frac{5}{2}, \pm\frac{1}{2})$	k_{\pm}^3	0	k_+	TBC		Linear	
				C_6	(4,1,1,4)	$(\pm\frac{3}{2}, \pm\frac{3}{2})$	k_{\pm}^3	0	k_{\pm}^3	TBC		Cubic	
τ_x	τ_0	τ_x	C_2/C_6	-	-	-	-	-	-	-	-		
			C_4	(2,0,1,3)	$(\pm\frac{3}{2}, \pm\frac{1}{2})$	k_{\pm}^2	0	k_+	TBC	BiO_2	Linear		
	τ_z	$i\tau_y$		C_2/C_4	-	-	-	-	-	-	-		
				C_6	(3,0,2,5)	$(\pm\frac{5}{2}, \pm\frac{1}{2})$	k_{\pm}^3	k_-^2	k_+	TBC	-	Linear	

TABLE III. Classification table of topological phase for D_{3h} . In the presence of C_3 symmetry, Dirac semimetals can only be obtained in the systems with $M_z = i\tau_y \otimes \sigma_z$. $H(k_z)$ is the Hamiltonian on k_z axis after considering reflection symmetry but without constraints by rotation symmetry.

Mirror operator	$H(k_z)$	C_n Constraint	Possible (p, q, r, s)	Total j	Dirac type
τ_0	$h_{\uparrow\uparrow} = a_{10}\tau_x + a_{23}\tau_y + a_{30}\tau_z$ $h_{\uparrow\downarrow} = a_{01} - ia_{02} + (a_{11} - ia_{12})\tau_x + (a_{31} - ia_{32})\tau_z$	$p \neq q \neq r$ $q \neq s$	-	-	-
τ_x	$h_{\uparrow\uparrow} = a_{10}\tau_x + a_{20}\tau_y + a_{33}\tau_z$ $h_{\uparrow\downarrow} = a_{01} - ia_{02} + (a_{11} - ia_{12})\tau_x - i(a_{21} - ia_{22})\tau_y$	$p \neq q \neq r$ $q \neq s$	-	-	-
$i\tau_y$	$h_{\uparrow\uparrow} = a_{13}\tau_x + a_{23}\tau_y + a_{33}\tau_z$ $h_{\uparrow\downarrow} = a_{01} - ia_{02}$	$p \neq q$	(2,0,0,2) (2,1,0,1)	$(\pm\frac{1}{2}, \pm\frac{1}{2})$ $(\pm\frac{1}{2}, \pm\frac{3}{2})$	TBC TBC
τ_z	$h_{\uparrow\uparrow} = a_{13}\tau_x + a_{20}\tau_y + a_{30}\tau_z$ $h_{\uparrow\downarrow} = a_{01} - ia_{02} - i(a_{21} - ia_{22})\tau_y + (a_{31} - ia_{32})\tau_z$	$p \neq q \neq r$ $q \neq s$	-	-	-

pendent of the creation of Dirac semimetal phase in bulk band structure.

Numerical calculation shows that the two crossing bands of Weyl line nodes in blue areas have different mirror eigenvalues, which protects the gap closing on the Weyl line nodes.

Weyl line nodes are protected when the crossing bands

have different mirror eigenvalues due to the absence of level repulsion. As is shown in FIG. 3.(c)(d), Weyl line nodes may emerge on various kinds of mirror plane.

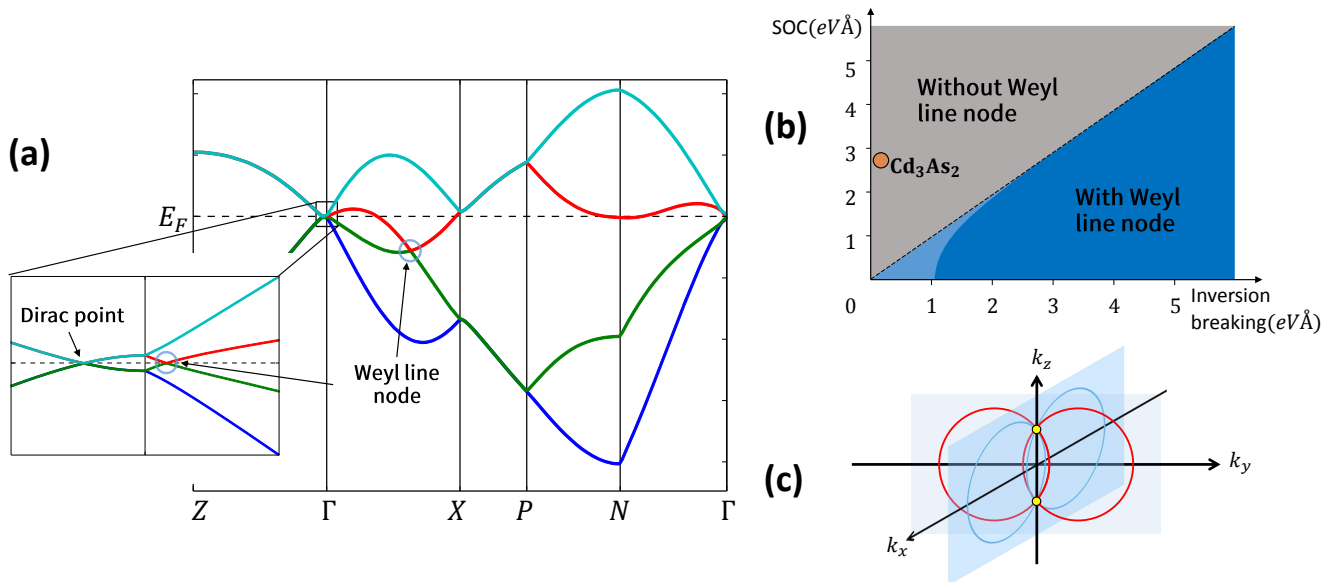


FIG. 2. (a) The electronic structure of C_{4v} system with SOC. The Dirac points and Weyl line nodes can exist simultaneously. The parameters are listed in the Appendix TABLE VI. (b) Phase diagram with respect to B_0 , D_0 and A_0 of C_{4v} system results from the Hamiltonian [Equation(11)] of $k \cdot p$ perturbation method. For all other parameters we fix them using the values fixed for Cd_3As_2 [18](see Appendix TABLE VI). The inversion breaking term is B_0 and SOC is described by D_0 . Weyl line nodes exist in the blue areas, among which the dark blue area represents the situation when the parameter $A_0 = 0.06\text{eV}$ (Cd_3As_2)[18] and the light blue area (partially covered by the dark one) for $A_0 = 0.00922\text{eV}$ (HgTe)[47]. (c) Schematic diagram of the distribution of Dirac points(yellow points) and Weyl line nodes(red or blue circles) in Brillouin zone. Dirac points locate on the interception of four Weyl line nodes.

II.4. Dirac and Weyl line nodes in mirror plane

Recently proposed by Fang, et al[23], Dirac line nodes in mirror plane emerge in systems with inversion symmetry, time reversal symmetry and reflection symmetry. The combination of inversion operation and reflection operation generates C_2 rotation perpendicular to mirror plane, which is covered by our framework. Due to the combination of inversion symmetry and TRS, two bands related by TRS actually stick together and make up a two-fold degenerate band.

When we study the Hamiltonian in the mirror plane, the mirror symmetry give $MH(k_x, k_y)|_{k_z=0}M^{-1} = H(k_x, k_y)|_{k_z=0}$. Therefore, if the conduction (valence) band consists of two bands with different mirror eigenvalues, the bands with the same (positive or negative) mirror eigenvalue from the conduction and valence band will have strong level repulsion and open up a gap (FIG. 3.(a)(b)). Otherwise when TRS-partner bands have the same mirror eigenvalues, the conduction band will have a different mirror eigenvalue from the valence band, and the level repulsion will be relaxed. The band crossing between them will create Dirac line nodes in the mirror plane. Thus Dirac line nodes in mirror plane can only be protected by the nonsymmorphic $M_z = \pm i\tau_y \otimes i\sigma_z$ (FIG. 3.(a)(b) and TABLE IV).

Different from Weyl line nodes in HgCr_2Se_4 [24] and $(\text{CdO})_2(\text{EuO})_2$ [26], we construct Weyl line nodes in the presence of TRS. Weyl line nodes are protected when

the crossing bands have different mirror eigenvalues. As is shown in FIG. 3.(c)(d) and TABLE IV, Weyl line nodes may emerge on various kinds of mirror plane because of its two-fold degeneracy nature. Whereas Dirac line nodes in mirror plane can only be protected by $M_z = \pm i\tau_y \otimes i\sigma_z$ which satisfies the requirement of mirror eigenvalues above. Note that DLN and WLN protected by mirror symmetry also apply to two-dimensional systems, because in three-dimensional systems we just take a plane into consideration by fixing k_z .

III. CONCLUSION

In this work we show that reflection symmetry can protect Dirac semimetal phase with or without inversion symmetry. We have classified Dirac semimetal in the systems preserving reflection symmetry, rotational symmetry and TRS. TABLE IV can be referred to for an overall possible protection of semimetal phases by reflection symmetry. There are two kinds of Dirac semimetals created via ABC and TBC. In C_2 and C_3 rotation invariant systems, Dirac semimetals can be created only via TBC. Whereas in C_4 and C_6 systems, Dirac semimetals can be created via not only ABC but also TBC. We also found that in C_{4v} point group system, Dirac semimetal phase can coexist with Weyl line nodes. Finally we show that DLN in mirror plane can be protected only by $M_z = i\tau_y \otimes i\sigma_z$ and WLN can be pro-

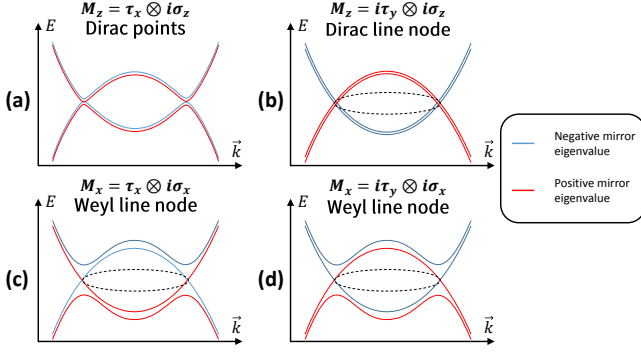


FIG. 3. Dirac or Weyl line nodes protected by reflection symmetry. Only $i\tau_y \otimes \sigma_z$ can protect Dirac line nodes while all kinds of mirror plane can protect Weyl line nodes. (a)(b)[23] are inversion preserving systems where Dirac line nodes may emerge and (c)(d) are inversion breaking systems where Weyl line nodes may emerge. (a) For mirror operators other than $i\tau_y \otimes i\sigma_z$ (e.g. $\tau_x \otimes i\sigma_z$), two bands with different mirror eigenvalues compose conduction (valence) band. Apart from two Dirac points, a gap between conduction and valence bands will open due to level repulsion. (b) For mirror $M_z = i\tau_y \otimes i\sigma_z$, conduction (valence) band consists of two bands with the same mirror eigenvalues. There isn't level repulsion between conduction and valence bands and the crossing of two bands generates a Dirac line node. The existence and classification of DLN by different reflection symmetries are shown in TABLE IV. (c)(d) For various kinds of mirrors (e.g. $i\tau_y \otimes i\sigma_x$ and $\tau_x \otimes i\sigma_x$), Weyl line nodes can be protected as long as the crossing bands have different mirror eigenvalues and so level repulsion doesn't happen (TABLE IV).

TABLE IV. The possible protected semimetal phases by reflection symmetry. The mirror operators with σ_x stands for mirror parallel to rotation axis and σ_z for mirror perpendicular to rotation axis. Dirac line nodes in mirror plane is denoted by DLN.

Mirror operator	ABC	TBC	WLN	DLN
$\tau_0 \otimes i\sigma_x$	✓		✓	
$\tau_x \otimes i\sigma_x$		✓	✓	
$i\tau_y \otimes i\sigma_x$		✓	✓	
$\tau_z \otimes i\sigma_x$	✓		✓	
$\tau_0 \otimes i\sigma_z$	✓		✓	
$\tau_x \otimes i\sigma_z$		✓	✓	
$i\tau_y \otimes i\sigma_z$		✓	✓	✓
$\tau_z \otimes i\sigma_z$	✓		✓	

tected by any mirror operator. These new classes of Dirac semimetals in inversion breaking and preserving systems can guide the search for novel materials with exotic quantum properties[48].

IV. ACKNOWLEDGMENTS

Xiao Zhang is support by the National Natural Science Foundation of China (No.11404413). Meng Hua and

Zihao Gao acknowledge financial support from Yat-sen school, Sun Yat-sen University.

V. APPENDIX

V.1. The constraint on Hamiltonian by TRS and rotational symmetry

In this section we first constrain the Hamiltonian with TRS and rotational symmetry. Then we impose rotational symmetry C_n to the whole system to determine the leading order of the elements in $h_{\uparrow\uparrow}(\vec{k})$ and $h_{\uparrow\downarrow}(\vec{k})$. The Hamiltonian and the basis we use here are the same as those in the main text. Time reversal symmetry will give constraints to the Hamiltonian $H(\vec{k})$: $H(-\vec{k}) = TH(\vec{k})T^{-1}$, where the time reversal operator $T = i\sigma_y K$. We will have[38]

$$H = \begin{pmatrix} h_{\uparrow\uparrow}(\vec{k}) & h_{\uparrow\downarrow}(\vec{k}) \\ -h_{\uparrow\downarrow}^*(-\vec{k}) & h_{\uparrow\uparrow}^*(-\vec{k}) \end{pmatrix}$$

At the same time, we know the parity of each coefficient with respect to momentum $a_{01,02,03,11,12,13,20,31,32,33}(-\vec{k}) = -a_{01,02,03,11,12,13,20,31,32,33}(\vec{k})$ and $a_{00,10,21,22,23,30}(-\vec{k}) = a_{00,10,21,22,23,30}(\vec{k})$. We set the rotation axis as k_z and choose the eigenstates of the rotation operator C_n as the basis of matrices. Then the matrix representation of C_n is

$$\begin{aligned} C_n &= \text{diag}[\alpha_p, \alpha_q, \alpha_r, \alpha_s] \\ &= \begin{pmatrix} e^{i\frac{2\pi}{n}(p+1/2)} & 0 & 0 & 0 \\ 0 & e^{i\frac{2\pi}{n}(q+1/2)} & 0 & 0 \\ 0 & 0 & e^{i\frac{2\pi}{n}(r+1/2)} & 0 \\ 0 & 0 & 0 & e^{i\frac{2\pi}{n}(s+1/2)} \end{pmatrix} \\ &= \begin{pmatrix} e^{i\pi(\frac{1+p+q}{n} + \frac{p-q}{n}\tau_z)} & 0 \\ 0 & e^{i\pi(\frac{1+r+s}{n} + \frac{r-s}{n}\tau_z)} \end{pmatrix} \end{aligned} \quad (2)$$

where $p, q, r, s \in \{0, 1, \dots, n-1\}$ and can be regarded as orbital angular momentum of different states. In general, C_n commute with TRS $[C_n, T] = 0$, thus p and r, q and s are related by:

$$\begin{aligned} \alpha_p &= \bar{\alpha}_r, \alpha_q = \bar{\alpha}_s \\ \exp[i\frac{2\pi}{n}(p+r+1)] &= 1, \exp[i\frac{2\pi}{n}(q+s+1)] = 1 \end{aligned} \quad (3)$$

Next we derive the constraint relations between rotational symmetry and elements of the Hamiltonian. The 2×2 block Hamiltonian $h_{\uparrow\uparrow}, h_{\uparrow\downarrow}$ can be expanded in the following way[49]:

$$\begin{aligned} h_{\uparrow\uparrow}(\vec{k}) &= f_0(\vec{k}) + f_+(\vec{k})\tau_+ + f_+(\vec{k})\tau_- + f_z(\vec{k})\tau_z \\ h_{\uparrow\downarrow}(\vec{k}) &= g_0(\vec{k}) + g_+(\vec{k})\tau_+ + g_-(\vec{k})\tau_- + g_z(\vec{k})\tau_z \end{aligned} \quad (4)$$

where $\tau_{\pm} = \tau_x \pm i\tau_y$, $f_{0,z}$ are real functions and f_+, g_0, g_z, g_{\pm} are complex functions. Then the rotational symmetry $C_n H(k_{\pm}, k_z) C_n^{-1} = H(k_{\pm} e^{\pm i2\pi/n}, k_z)$ gives the constraints of elements of the Hamiltonian:

$$\begin{aligned} f_z(k_{\pm}, k_z) &= f_z(k_{\pm} e^{\pm i2\pi/n}, k_z) \\ \exp\left[i\frac{2\pi}{n}(p-q)\right] f_+(k_{\pm}, k_z) &= f_+(k_{\pm} e^{\pm i2\pi/n}, k_z) \\ \exp\left[i\frac{2\pi}{n}(p-r)\right] g_{0+z}(k_{\pm}, k_z) &= g_{0+z}(k_{\pm} e^{\pm i2\pi/n}, k_z) \\ \exp\left[i\frac{2\pi}{n}(q-s)\right] g_{0-z}(k_{\pm}, k_z) &= g_{0-z}(k_{\pm} e^{\pm i2\pi/n}, k_z) \\ \exp\left[i\frac{2\pi}{n}(q-r)\right] g_{\pm}(k_{\pm}, k_z) &= g_{\pm}(k_{\pm} e^{\pm i2\pi/n}, k_z) \end{aligned} \quad (5)$$

where $k_{\pm} = k_x \pm ik_y$, $g_{0\pm z} = g_0 \pm g_z$.

On k_z axis, these constraints become,

$$\begin{aligned} f_z(k_z) &= f_z(k_z) \\ \exp\left[i\frac{2\pi}{n}(p-q)\right] f_+(k_z) &= f_+(k_z) \\ \exp\left[i\frac{2\pi}{n}(p-r)\right] g_{0+z}(k_z) &= g_{0+z}(k_z) \\ \exp\left[i\frac{2\pi}{n}(q-s)\right] g_{0-z}(k_z) &= g_{0-z}(k_z) \\ \exp\left[i\frac{2\pi}{n}(q-r)\right] g_{\pm}(k_z) &= g_{\pm}(k_z) \end{aligned} \quad (6)$$

After considering all other symmetric relations (e.g. reflection symmetry in V.3), if non-diagonal f, g terms aren't eliminated on k_z axis, the corresponding (p,q,r,s) pairs (f_+ to p, q , $g_0 + g_z$ to p, r , $g_0 - g_z$ to q, s , g_{\pm} to q, r) should be unequal to obtain Dirac points. For example, if f_+ exists on k_z axis, we should apply $p \neq q$ or a gap will open on k_z axis.

In order to get the dispersion relation near Dirac points, we should change the f, g terms into a more explicit form. The matrix elements can be expanded as polynomial[49]:

$$f(k_+, k_-) = \sum_{n_1, n_2} A_{n_1 n_2} k_+^{n_1} k_-^{n_2}. \quad (7)$$

Combined with the constraint relations (5), we obtain

$$\begin{aligned} e^{i2\pi(p-q)/n} f(k_+, k_-) &= f(k_+ e^{i2\pi/n}, k_- e^{-i2\pi/n}) \\ &= \sum_{n_1, n_2} \exp\left[i\frac{2\pi}{n}(n_1 - n_2)\right] A_{n_1 n_2} k_+^{n_1} k_-^{n_2} \end{aligned} \quad (8)$$

where $A_{n_1 n_2}$ is a complex coefficient. To satisfy above equations, the phase factors must cancel each other, i.e. $n_1 - n_2 = (p - q) \bmod n$. We choose the leading order terms to complete TABLE I and TABLE II. For example, in C_4 system with $p = 3$ and $q = 2$, the constraint relation of f_+ term is,

$$\exp\left(i\frac{2\pi}{n}\right) f_+(k_{\pm}, k_z) = f_+(k_{\pm} e^{\pm i2\pi/n}, k_z) \quad (9)$$

Obviously the leading order term is given by $n_1 = 1, n_2 = 0$, and so we can replace the f_+ term by $A_{1,0} k_+$, neglecting the higher order terms.

V.2. Details about the classification of reflection symmetry operators

We study the general classification of reflection symmetry operators. The matrix representation of reflection symmetry can be decomposed to orbital space and angular momentum space. In spin space, mirror operator is a two-fold rotation perpendicular to the mirror plane \hat{n} : $R_{\pi/2}(\hat{n}) = e^{-i\hat{\sigma}j \cdot \hat{n}\pi/2}$, where j indicates the half-integer spin momentum. At the same time, mirror operators should satisfy the following constraints: (1) $[M, T] = 0$, (2) $M^+ M = 1$, (3) $MM = e^{i\phi}$. The reflection symmetry operators can take four possible forms: (A) $M_k = \pm\tau_0 \otimes i\sigma_k$, (B) $M_k = \pm\tau_z \otimes i\sigma_k$, (C) $M_k = \pm\tau_x \otimes i\sigma_k$ and (D) $M_k = \pm i\tau_y \otimes i\sigma_k$ ($k = x, z$, see Appendix), among which (C, D) represent glide mirror symmetry.

As is shown in FIG. 1., physically there are two classes of mirrors, the mirror parallel to rotation axis and the mirror perpendicular to the rotation axis, respectively correspond to $k = x$ and $k = z$ above.

We can now give the physical interpretation of these mirror operators below, where A/B represent two inequivalent atom sites (see FIG. 1), $|P_{\pm}\rangle = |P_x\rangle \pm i|P_y\rangle$, and \uparrow, \downarrow represent spin:

1. We set the four basis as $(|P_{A+\uparrow}\rangle, |P_{A-\uparrow}\rangle, |P_{A-\downarrow}\rangle, |P_{A+\downarrow}\rangle)$. Then the yz -plane mirror operation interchange P_+, P_- and \uparrow, \downarrow , i.e. the mirror operation $M_x : |P_{A+\downarrow}\rangle \rightarrow -i|P_{A-\uparrow}\rangle, |P_{A+\uparrow}\rangle \rightarrow -i|P_{A-\downarrow}\rangle, |P_{A-\uparrow}\rangle \rightarrow -i|P_{A+\downarrow}\rangle, |P_{A-\downarrow}\rangle \rightarrow -i|P_{A+\uparrow}\rangle$. The matrix representation of mirror operator is $M_x = -\tau_0 \otimes i\sigma_x$.
2. We set the four basis as $(|P_{A+\downarrow}\rangle, |P_{B+\downarrow}\rangle, -|P_{A-\uparrow}\rangle, -|P_{B-\uparrow}\rangle)$. A glide plane operator can have the following transformation $M_x : |P_{A+\downarrow}\rangle \rightarrow -i|P_{B-\uparrow}\rangle, |P_{B+\downarrow}\rangle \rightarrow -i|P_{A-\uparrow}\rangle, |P_{A-\uparrow}\rangle \rightarrow -i|P_{B+\downarrow}\rangle, |P_{B-\uparrow}\rangle \rightarrow -i|P_{A+\downarrow}\rangle$. Therefore the matrix representation of mirror operator is $M_x = \pm\tau_x \otimes i\sigma_x$.

In general basis for this mirror operator can be constructed as following: There are two inequivalent sites (A and B) and the distance between them is \vec{t} . This transformation can be provided by defining: $|P_{A\pm\uparrow(\downarrow)}\rangle = e^{\pm i\vec{r}\cdot\vec{K}} u_{A\pm\uparrow(\downarrow)}, |P_{B\pm\uparrow(\downarrow)}\rangle = e^{\pm iM\vec{r}\cdot\vec{K}} u_{B\pm\uparrow(\downarrow)}$, where \vec{K} denote the point in Brillouin zone, $u_{A\pm}(M\vec{r} + \vec{t}) e^{\pm i\vec{t}\cdot\vec{K}} = u_{B\pm}(\vec{r})$ and $u_A(\vec{r} + M\vec{t} + \vec{t}) = u_A(\vec{r})$. $M_z : \vec{r} \rightarrow M\vec{r} + \vec{t}$, where M is a symmorphic mirror operation acting on \vec{k} space and $\vec{K} \cdot (M\vec{t} + \vec{t}) = 2\pi n$. For BiO_2 of space group #227, the Dirac point appears in the X point of its Brillouin zone with reflection symmetry belong to this case.

3. We set the four basis as $(|P_{A+\uparrow}\rangle, |P_{A+\downarrow}\rangle, |P_{A-\downarrow}\rangle, -|P_{A-\uparrow}\rangle)$ yz -plane mirror operation $M_x : |P_{A+\downarrow}\rangle \rightarrow -i|P_{A-\uparrow}\rangle, |P_{A+\uparrow}\rangle \rightarrow -i|P_{A-\downarrow}\rangle, |P_{A-\uparrow}\rangle \rightarrow -i|P_{A+\downarrow}\rangle, |P_{A-\downarrow}\rangle \rightarrow -i|P_{A+\uparrow}\rangle$ has a matrix form $M_x = -\tau_z \otimes i\sigma_x$.
4. We set the four basis as $(|P_{A+\downarrow}\rangle, |P_{B+\downarrow}\rangle, -|P_{A-\uparrow}\rangle, -|P_{B-\uparrow}\rangle)$. The mirror operation on xy -plane writes $M_z : |P_{A+\downarrow}\rangle \rightarrow i|P_{B+\downarrow}\rangle, |P_{B+\downarrow}\rangle \rightarrow -i|P_{A+\downarrow}\rangle, |P_{A-\uparrow}\rangle \rightarrow -i|P_{B-\uparrow}\rangle, |P_{B-\uparrow}\rangle \rightarrow i|P_{A-\uparrow}\rangle$, with a matrix representation $M_z = i\tau_y \otimes i\sigma_z$. There are two inequivalent sites(A and B) and the distance between them is \vec{t} . This transformation can be provided by defining: $|P_{A\pm\uparrow(\downarrow)}\rangle = e^{\pm i\vec{r}\cdot\vec{K}}u_{A\pm\uparrow(\downarrow)}, |P_{B\pm\uparrow(\downarrow)}\rangle = e^{\pm iM\vec{r}\cdot\vec{K}}u_{B\pm\uparrow(\downarrow)}$, where \vec{K} denote the point in Brillouin zone, $u_{A\pm}(M\vec{r} + \vec{t})e^{\pm i\vec{t}\cdot\vec{K}} = u_{B\pm}(\vec{r})$ and $u_A(\vec{r} + M\vec{t} + \vec{t}) = u_A(\vec{r})$. $M_z : \vec{r} \rightarrow M\vec{r} + \vec{t}$, where M is a symmorphic mirror operation acting on \vec{k} space and $\vec{K} \cdot (M\vec{t} + \vec{t}) = (2n + 1)\pi$.

V.3. The constraint on Hamiltonian by reflection symmetry and rotational symmetry

Now we show how the Hamiltonian in k_z axis is constrained by reflection symmetry and rotational symmetry:

Mirror plane parallel to k_z axis: First we set the mirror plane as yz plane and the mirror operator as M_x . The combination of M_x and n -fold rotation operation generate $n-1$ more mirror planes and therefore all these mirror operators can be denoted as $M_k = C_n^k M_x (k = 0, 1, \dots, n-1)$. These mirror planes cross on k_z axis and confine the Hamiltonian in k_z axis. For each M_k , there's commutation relation $M_k H(k_z) M_k^{-1} = H(k_z)$. For the basis satisfying constraint relations (6), when $M_x = \tau_0/\tau_z \otimes i\sigma_x$, the Hamiltonian becomes $H(k_z) = \text{diag}[a_0 + a_{30}, a_0 - a_{30}, a_0 + a_{30}, a_0 - a_{30}]$; when $M_x = \tau_x/i\tau_y \otimes i\sigma_x$, the Hamiltonian becomes $H(k_z) = \text{diag}[a_0 + a_{33}, a_0 - a_{33}, a_0 + a_{33}, a_0 - a_{33}]$. It is notable that at TRIM all a terms with odd parity eliminated due to the relation $[H, T] = 0$ and only $a_{00}, a_{10}, a_{30}, a_{21}, a_{22}, a_{23}$ survive. Therefore, the constraints on (p, q, r, s) are lessen in TBC. All the results of the physical properties of Dirac semimetal are shown in TABLE I.

Mirror plane perpendicular to k_z axis: First we set the mirror plane as xy plane and the mirror operator as M_z . Along the k_z axis, the reflection symmetry is $M_z H(k_z) M_z^{-1} = H(-k_z)$. Combined with C_2, C_4, C_6 rotational symmetry, reflection symmetry can create inversion symmetry $P = M_z \hat{C}_2$. The rotation operator for orbital space is $C_n = i \exp(i\pi \frac{1+p+q}{n}) \exp(i\pi \frac{p-q}{n} \tau_z) = i \exp(i\pi \frac{1+p+q}{n}) [\cos \frac{\pi}{n}(p-q) + i\tau_z \sin \frac{\pi}{n}(p-q)]$. Two-fold rotation is $\hat{C}_2 = \cos \theta \tau_0 + \sin \theta \tau_z$ where $\theta = \frac{\pi}{2}(p-q)$. If $p-q = 0, 2, 4$, then $\hat{C}_2 = \pm\tau_0$. These conditions can be satisfied when $p = q$ for C_2 symmetry, when $p = q$ or $p = q + 2$ for C_4 symmetry, when $p = q,$

$p = q + 2$ or $p = q + 4$ for C_6 symmetry. If $p - q = 1, 3, 5$, then $\hat{C}_2 = \pm\tau_z$. These conditions can be satisfied when $p = 1, q = 0$ for C_2 symmetry, when $p = q + 1$ or $p = q + 3$ for C_4 symmetry, when $p = q + 1, p = q + 3$ or $p = q + 5$ for C_6 symmetry. The symmetry constraints with TRS along k_z axis are $M_z H(k_z) M_z^{-1} = TH(k_z)T^{-1}$ and $PH(k_z)P^{-1} = TH(k_z)T^{-1}$. After $[H, T] = 0$ at TRIM and constraint relations(6) are applied, all situations protecting Dirac points are shown in TABLE II, holding the same result with Yang and Nagaosa[38] when $P = \pm\tau_0, \pm\tau_z, \pm\tau_x$. Note that there are additional conditions for inversion symmetry $P\Gamma_\mu P^{-1} = \pm\Gamma_\mu (\mu = 03, 30, 33)$ [38], the case for mixed mirror operator is thus eliminated. When $P = \pm i\tau_y$ the system can also generate Dirac points. For C_3 symmetry, the system does not have inversion symmetry. We only have symmetry constraints $m_z H(k_z) m_z^{-1} = TH(k_z)T^{-1}$ and $[H, T] = 0$ at TRIM and the result is shown in TABLE III.

V.4. $k \cdot p$ model

In this section, we use the four band model to describe the effective Hamiltonian of material with point group C_{4v} such as Cd_3As_2 . We write the 4×4 effective Hamiltonian generally as:

$$H_{\text{eff}} = \sum_{i,j=0}^3 d_{ij}(k) \Gamma_{ij} \quad (10)$$

where $\Gamma_{ij} = \tau_i \sigma_j$. The basis of effective Hamiltonian are four angular momentum eigenstates $|+\frac{1}{2}\rangle, |+\frac{3}{2}\rangle, |-\frac{1}{2}\rangle$ and $|-\frac{3}{2}\rangle$.

Then we investigate the representations of Γ matrices and k polynomials with three symmetric operations: the four-fold rotation along Z axis \hat{C}_4 , the vertical reflection \hat{m}_v and the dihedral reflection $\hat{m}_d = \hat{C}_4 \hat{m}_v$.

The matrix operation of symmetric operators are: (1) $U(\hat{C}_4) = R_{\frac{1}{2}}(\hat{C}_4) \oplus R_{\frac{3}{2}}(\hat{C}_4)$, (2) $U(\hat{m}_v) = R_{\frac{1}{2}}(\hat{m}_v) \oplus R_{\frac{3}{2}}(\hat{m}_v)$, and (3) $U(\hat{m}_d) = U(\hat{m}_v)U(\hat{C}_4)$, where $R_j(\hat{C}_4) = \exp(i\frac{\pi}{2}j\sigma_z), R_j(\hat{m}_v) = \exp(i\frac{\pi}{2}j\sigma_x)$.

The operators act on the k polynomials $d_{ij}(k)$ as : (1) $\hat{C}_4 : k_x \rightarrow -k_y, k_y \rightarrow k_x, k_z \rightarrow k_z$, (2) $\hat{m}_v : k_x \rightarrow -k_x, k_y \rightarrow k_y, k_z \rightarrow k_z$, (3) $\hat{m}_d : k_x \rightarrow k_y, k_y \rightarrow k_x, k_z \rightarrow k_z$.

The representations of Γ matrices and k polynomials $d(k)$ are shown in TABLE V. By assembling the Γ matrices and $d(k)$ with the same representation and time-reversal eigenvalue we obtain our effective Hamiltonian:

$$H_{\text{eff}}(\vec{k}) = \epsilon(\vec{k}) + \begin{pmatrix} A(\vec{k}) & -D(\vec{k})k_+ & B_+k_- & -C(\vec{k}) \\ -D^*(\vec{k})k_- & -A(\vec{k}) & C(\vec{k}) & B_-k_+ \\ B_+k_+ & C^*(\vec{k}) & A(\vec{k}) & D(\vec{k})k_- \\ -C^*(\vec{k}) & B_-k_- & D^*(\vec{k})k_+ & -A(\vec{k}) \end{pmatrix} \quad (11)$$

where $\epsilon(\vec{k}) = E_0 + E_1 k_+ k_- + E_2 k_z^2, A(\vec{k}) = A_0 + A_1 k_+ k_- +$

TABLE V. The representations of Γ matrices and \mathbf{k} polynomials

Reps	Γ matrices	$\mathbf{d}(\mathbf{k})$	\mathbf{T}
$\tilde{\Gamma}_1$	Γ_{00}, Γ_{30}	$1, k_x^2 + k_y^2, k_z^2$	+
$\tilde{\Gamma}_1$	-	k_z	-
$\tilde{\Gamma}_2$	Γ_{03}, Γ_{33}	-	-
$\tilde{\Gamma}_3$	Γ_{22}	$k_x^2 - k_y^2$	+
$\tilde{\Gamma}_3$	Γ_{12}	-	-
$\tilde{\Gamma}_4$	Γ_{21}	$k_x k_y$	+
$\tilde{\Gamma}_4$	Γ_{11}	-	-
$\tilde{\Gamma}_5$	$(\Gamma_{10}, \Gamma_{23})$	$(k_x k_z, k_y k_z)$	+
$\tilde{\Gamma}_5$	$(\Gamma_{32}, \Gamma_{01}), (\Gamma_{02}, \Gamma_{31}), (\Gamma_{20}, -\Gamma_{13})$	(k_x, k_y)	-

TABLE VI. Parameters for the 4×4 effective Hamiltonian. Most parameters can be referred to from Jeon, Sangjun, et al[18].

$E_0(\text{eV})$	-0.219	$B_0(\text{eV}\text{\AA})$	5
$E_1(\text{eV}\text{\AA}^2)$	-30	$B_1(\text{eV}\text{\AA})$	0
$E_2(\text{eV}\text{\AA}^2)$	-16	$C_0(\text{eV}\text{\AA}^2)$	0
$A_0(\text{eV})$	-0.060	$C_1(\text{eV}\text{\AA}^2)$	0
$A_1(\text{eV}\text{\AA}^2)$	18	$D_0(\text{eV}\text{\AA})$	-2.75
$A_2(\text{eV}^2\text{\AA}^2)$	96	$D_1(\text{eV}\text{\AA}^2)$	0
$A_{20}(\text{eV}^2)$	0.050		

$\sqrt{A_2 k_z^2 + A_{20}^2}$, $B_{\pm} = \pm B_0 + B_1$, $C(\vec{k}) = \frac{C_0}{2}(k_+^2 + k_-^2) + \frac{i}{4}C_1(k_+^2 - k_-^2)$, $D(\vec{k}) = D_0 + iD_1 k_z$, and $k_{\pm} = k_x \pm ik_y$.

The Hamiltonian (11) shows the possibility of coexistence of 3D Dirac points and Weyl line nodes. By choosing proper parameters shown in TABLE VI (Only B_0 is different from Cd_3As_2) we can verify our statement through the band structure FIG. 2.(a). FIG. 2.(a) is accomplished with the substitutions: $k_i \rightarrow \frac{1}{L_i} \sin(k_i L_i)$, $k_i^2 \rightarrow \frac{2}{L_i^2} [1 - \cos(k_i L_i)]$ for a periodic lattice, where $L_x = L_y = a = 12.67\text{\AA}$ and $L_z = c = 25.48\text{\AA}$ [17].

In order to solve Weyl line nodes, it is convenient to neglect the symmetric terms $\epsilon(\vec{k})$ and some parameters B_1, C_0, C_1, D_1 as is shown in TABLE VI. Therefore, explicit calculation gives the equation of Weyl line nodes:

$$(B_0^2 - D_0^2)k_x^2 = \left[A_0 + A_1 k_x^2 + \sqrt{A_2 k_z^2 + A_{20}^2} \right]^2 \quad (12)$$

This is schematically shown in FIG. 2.(c).

In FIG. 2, the B_1, C_0, C_1, D_1 terms are neglected. B_0 and D_0 are two main parameters determining whether there is a gap or Weyl line nodes in BZ. The phase diagram of B_0 and D_0 is shown in FIG. 2.(b). The critical line where Weyl line nodes appear and disappear is close to the line $D_0 = B_0$, but B_0 is actually slightly larger than D_0 , which can be shown more clearly with a smaller A_0 [see FIG. 2.(b) the dark blue area]. On the critical line, the two bands pull apart and the Weyl line nodes eventually annihilate accompanied by opening a gap.

-
- [1] X.-L. Qi and S.-C. Zhang, *Phys. Today* 63, 33(2010).
- [2] X.-L. Qi and S.-C. Zhang, *Rev. Mod. Phys.* 83,1057 (2011).
- [3] M. Hasan and C. Kane, *Rev. Mod. Phys.* 82, 30453067 (2010).
- [4] C.-X. Liu, X.-L. Qi, H. Zhang, X. Dai, Z. Fang, and S.-C. Zhang, *Phys. Rev. B* 82, 045122 (2010).
- [5] K. S. Novoselov, A. K. Geim, S. V. Morozov, D. Jiang, M. I. Katsnelson, I. V. Grigorieva, S. V. Dubonos and A. A. Firsov, *Nature* 438, 7065 (2005).
- [6] Y. Zhang, Y.-W. Tan, H. L. Stormer and P. Kim, *Nature* 438, 04235 (2005).
- [7] S. Young, S. Zaheer, J. Teo, C. Kane, E. Mele, and A. Rappe, *Phys. Rev. Lett.* 108, 140405 (2012).
- [8] S. Young and C. Kane, arXiv: 1504.07977 (2015).
- [9] Z. Wang, Y. Sun, X.-Q. Chen, C. Franchini, G. Xu, H. Weng, X. Dai, and Z. Fang, *Phys. Rev. B* 85, 195320(2012).
- [10] Y. Kim, B. Wieder, C. Kane, and A. Rappe, *Phys. Rev. Lett.* 115, 036806 (2015).
- [11] E. Burstein, A. H. MacDonald and P. J. Stiles. *Contemporary Concepts of Condensed Matter Science Topological Insulators Volume 6* (Elsevier 2013).
- [12] C.-X. Liu, P. Ye, and X.-L. Qi, *Phys. Rev. B* 87, 235306 (2013).
- [13] T Morimoto and A Furusaki, *Phys. Rev. B* 89, 235127 (2014).
- [14] R. Yu, H. Weng, Z. Fang, X. Dai, and X. Hu, arXiv: 1504. 04577 (2015).
- [15] B. Bttner, C. Liu, G. Tkachov, E. Novik, C. Brne, H. Buhmann, E. Hankiewicz, P. Recher, B. Trauzettel, S. Zhang, and L. Molenkamp, *Nat. Phys.* 7, 418 (2011).
- [16] Z. Wang, H. Weng, Q. Wu, X. Dai, and Z. Fang, *Phys. Rev. B* 88, 125427 (2013).
- [17] M. Neupane, S.-Y. Xu, R. Sankar, N. Alidoust, G. Bian, C. Liu, I. Belopolski, T.-R. Chang, H.-T. Jeng, H. Lin, A. Bansil, F. Chou, and M. Hasan, *Nat. Comms.* 5, 4786(2014).
- [18] S. Jeon, B. Zhou, A. Gyenis, B. Feldman, I. Kimchi, A. Potter, Q. Gibson, R. Cava, A. Vishwanath, and A. Yazdani, *Nat. Mater.* 13, 851 (2014).
- [19] Z. Liu, J. Jiang, B. Zhou, Z. Wang, Y. Zhang, H. Weng, D. Prabhakaran, S.-K. Mo, H. Peng, P. Dudin, T. Kim, M. Hoesch, Z. Fang, X. Dai, Z. Shen, D. Feng, Z. Hussain, and Y. Chen, *Nat. Mater.* 13, 677 (2014).
- [20] M. Ali, Q. Gibson, S. Jeon, B. Zhou, A. Yazdani, and R. Cava, *Inorg. Chem.* 53, 4062 (2014).
- [21] Z. K. Liu, B. Zhou, Y. Zhang, Z. J. Wang, H. M. Weng, D. Prabhakaran, S.-K. Mo, Z. X. Shen, Z. Fang, X. Dai, Z. Hussain, and Y. L. Chen, *Science* 343, 864 (2014).
- [22] M. Zeng, C. Fang, G. Chang, Y.-A. Chen, T. Hsieh, A. Bansil, H. Lin, and L. Fu, arXiv:1504. 03492 (2015).
- [23] C. Fang, Y. Chen, H.-Y. Kee, and L. Fu, arXiv: 1506.03449 (2015).
- [24] G. Xu, H. Weng, Z. Wang, X. Dai, and Z. Fang, *Phys. Rev. Lett.* 107, 186806 (2011).
- [25] X. Wan, A.-M. Turner, A. Vishwanath, and S.-Y. Savrasov, *Phys. Rev. B* 83, 205101 (2011).
- [26] H. Zhang, J. Wang, G. Xu, Y. Xu, and S.-C. Zhang, *Phys. Rev. Lett.* 112, 096804 (2014).
- [27] H. Weng, C. Fang, Z. Fang, B. A. Bernevig, and X. Dai, *Phys. Rev. X* 5, 011029 (2015).
- [28] S.-M. Huang, S.-Y. Xu, I. Belopolski, C.-C. Lee, G. Chang, B. Wang, N. Alidoust, G. Bian, M. Neupane, A. Bansil, H. Lin, and M. Hasan, *Nat. Comms.* 6, 7373 (2015).
- [29] S.-Y. Xu, I. Belopolski, N. Alidoust, M. Neupane, G. Bian, C. Zhang, R. Sankar, G. Chang, Z. Yuan, C.-C. Lee, S.-M. Huang, H. Zheng, J. Ma, D. Sanchez, B. Wang, A. Bansil, F. Chou, P. Shibayev, H. Lin, S. Jia, and M. Hasan, *Science* 349, 613 (2015).
- [30] B. Q. Lv, H. M. Weng, B. B. Fu, X. P. Wang, H. Miao, J. Ma, P. Richard, X. C. Huang, L. X. Zhao, G. F. Chen, Z. Fang, X. Dai, T. Qian, and H. Ding, arXiv:1502.04684 (2015).
- [31] B. Q. Lv, N. Xu, H. M. Weng, J. Z. Ma, P. Richard, X. C. Huang, L. X. Zhao, G. F. Chen, C. Matt, F. Bisti, V. Stokov, J. Mesot, Z. Fang, X. Dai, T. Qian, M. Shi, and H. Ding, arXiv:1503.09188 (2015).
- [32] X. Yang, Y. Li, Z. Wang, Y. Zhen, and Z.-a. Xu, arXiv:1506.02283 (2015).
- [33] L. Yang, Z. Liu, Y. Sun, H. Peng, H. Yang, T. Zhang, B. Zhou, Y. Zhang, Y. Guo, M. Rahn, D. Prabhakaran, Z. Hussain, S.-K. Mo, C. Felser, B. Yan, and Y. Chen, arXiv:1507.00521 (2015).
- [34] C. Shekhar, A. K. Nayak, Y. Sun, M. Schmidt, M. Nicklas, I. Leermakers, U. Zeitler, Y. Skourski, J. Wosnitza, Z. Liu, Y. Chen, W. Schnelle, H. Borrmann, Y. Grin, C. Felser and B.-H. Yan, *Nat. Phys.* 3327 (2015).
- [35] C. Shekhar, F. Arnold, S.-C. Wu, Y. Sun, M. Schmidt, N. Kumar, A.-G. Grushin, J.-H. Bardarson, R. D. dos Reis, M. Naumann, M. Baenitz, H. Borrmann, M. Nicklas, E. Hassinger, C. Felser, and B.-H. Yan, arXiv:1506.06577 (2015).
- [36] C. Zhang, Z. Yuan, S. Xu, Z. Lin, B. Tong, M. Hasan, J. Wang, C. Zhang, and S. Jia, arXiv:1502.00251 (2015).
- [37] X. Huang, L. Zhao, Y. Long, P. Wang, D. Chen, Z. Yang, H. Liang, M. Xue, H. Weng, Z. Fang, X. Dai, and G. Chen, arXiv:1503.01304 (2015).
- [38] B.-J. Yang and N. Nagaosa, *Nat. Comms.* 5, 4898 (2014).
- [39] C.-K. Chiu, J. Teo, A. Schnyder, and S. Ryu, arXiv:1505.03535 (2015).
- [40] C.-K. Chiu, and A. Schnyder, arXiv:1408.4642 (2014).
- [41] B. Andrei Bernevig and Taylor L. Hughes. *Topological insulators and topological superconductors* (Princeton 2013).
- [42] L. Fu, C. Kane, and E. Mele, *Phys. Rev. Lett.* 98, 106803 (2007).
- [43] L. Fu and Kane, *Phys. Rev. B* 76, 045302 (2007).
- [44] Fu, L. *Phys. Rev. Lett.* 106, 106802 (2011).
- [45] T.-H. Hsieh, H. Lin, J. Liu, W. Duan, A. Bansil and L. Fu, *Nat. Comms.* 3, 982 (2012).
- [46] J.A. Steinberg, S.M. Young, S. Zaheer, C.L. Kane, and E.J. Mele, *Phys. Rev. Lett.* 112, 036403 (2014).
- [47] B. Bernevig, T. Hughes, and S.-C. Zhang, *Science* 314, 1757 (2006).
- [48] S. A. Yang, H. Pan, and F. Zhang, *Phys. Rev. Lett.* 113, 046401 (2014).
- [49] C. Fang, M. Gilbert, X. Dai, and A. Bernevig, *Phys. Rev. Lett.* 108, 266802 (2012).